

Computation of Scale-Independent Surface Roughness of Individual Mountains

***Dinesh Sathyamoorthy**

Science and Technology Research Institute for Defence (STRIDE), Ministry of Defence,
Malaysia.

Prof. Ir. Dr. Ahmad Fadzil Mohamad Hani

Department of Electrical and Electronics Engineering, Universiti Teknologi Petronas,
Malaysia.

Dr. Vijanth Sagayan a/l Asirvadam

Department of Electrical and Electronics Engineering, Universiti Teknologi Petronas,
Malaysia.

***Corresponding author**

Address: Science and Technology Research Institute for Defence (STRIDE), Taman Bukit
Mewah Fasa 9, 43000 Kajang, Selangor, Malaysia.

E-mail: dinsat60@hotmail.com

Abstract

Surface roughness is a useful tool for terrain analysis as it reflects numerous geophysical parameters, such as landform characteristics, distribution of crenulations and degree of erosivity. Hence, in the past few decades, the quantitative computation of surface roughness of terrains for the purposes of numerical surface study has received increasing attention. A number of algorithms have been employed to compute scale-dependant surface roughness of terrains, including RMS height, plane fitting, Fourier analysis and high-order statistics. These algorithms, which operate at singular scales of measurement, provide scale-dependant roughness parameters. In an earlier research effort, we proposed a procedure to compute a scale-independent surface roughness parameter from digital elevation models (DEMs). In this paper, this procedure is extended to perform the computation of the surface roughness of individual mountains extracted from DEMs. Mathematical morphology is employed to extract the mountains of the DEM. The lifting scheme is used to generate multiscale DEMs. The mask of pixels modified in each mountain object at each scale is computed by performing the intersection operation between the mountain object and the mask of pixels modified at each scale. The normalized probability functions for each mountain object are computed as the ratio of the area of pixels modified in the mountain object at each scale to the area of the mountain object. The computed normalized probability functions are used to compute the scale-independent average roughness of the mountain objects due to the distribution of convex and concave regions averaged over the mountain objects. As compared to available scale-dependant methodologies, the proposed methodology provides a more informative surface roughness parameter of mountains over varying scales by allowing for a more accurate quantification of the corresponding region's convexity/concavity, distinguishing between shallow and deep incisions. It is observed that the larger the area of the mountain object, the higher is its surface roughness.

Keywords: mountains, multiscale digital elevation models (DEMs), lifting scheme, convex and concave regions, normalized distribution function, surface roughness.

1 Introduction

Roughness is a measure of the texture of a surface. It is quantified by the vertical deviations of a real surface from its ideal form. If these deviations are large, the surface is rough; if they are small, the surface is smooth. Surface roughness is a useful tool for terrain analysis as it reflects numerous geophysical parameters, such as landform characteristics, distribution of crenulations and degree of erosivity. Hence, in the past few decades, the quantitative computation of surface roughness of terrains for the purposes of numerical surface study has received increasing attention.

A number of algorithms have been employed to compute surface roughness of terrains; a summary can be found in Shepard et al. (2001) and Li et al. (2005). The most commonly used roughness parameter, and the easiest to obtain, is the root-mean-square (RMS) height, or the standard deviation of heights above the mean (Brock, 1983; Bennett, 1992; Yokota et al., 2008). The profile is first detrended by subtracting a best fit linear function from the data, leaving a series of heights with a mean value of zero. This approach is insensitive to amplitude differences and is not a good frequency discriminator, and hence, is unable to provide an accurate surface roughness parameter. An alternative approach is to fit a plane to a surface, and use the error as an estimate of the surface roughness (Wilcox and Gennery, 1987). In the case of two sinusoidal surfaces of differing frequencies, plane fitting suffers from a fundamental shortcoming by producing the same roughness estimation. Stone and Dugundji (1965) propose a method of computing surface roughness using Fourier analysis. This method measures roughness along specific directions of a surface, and includes amplitude, frequency and autocorrelation terms. This approach provides surface roughness parameters that have consistent representation in the frequency domain. However, as it depends on the direction of measurement, it is influenced by the rotation and translation of the surface. The slope and intercept of the logarithmic plot of the power spectrum of the terrain profile is reported as a roughness parameter by van Zyl et al. (1991). However, there is no simple correspondence between the intercept or the slope of the logarithmic plot of the power spectrum and commonly used roughness measures. Other reported roughness measures, developed to overcome these shortfalls, include effective slope (Miller and Parsons, 1990; Campbell and Garvin, 1993), autocorrelation length (Turcotte, 1997), radiosity models (Li et al., 1998), median and absolute slope (Kreslavsky and Head, 1999), granulometry (Tay et al., 2005), high-order statistics (Nikora, 2005), and extended Kalman

filtering (Dabrowski and Banaszkiwicz, 2008). These algorithms, which operate at singular scales of measurement, provide scale-dependant roughness parameters.

Dinesh et al. (2008) propose a procedure to compute a scale-independent surface roughness parameter from digital elevation models (DEMs). First, multiscale DEMs are generated using the lifting scheme. The area of pixels modified at each scale is computed. The computed areas are divided with the area of the DEM to obtain the normalized probability functions, which are used to compute the average size of convex and concave regions in the DEM, and the scale-independent average roughness of the terrain of the DEM due to the distribution of convex and concave regions in the terrain.

In this paper, the procedure proposed in Dinesh et al. (2008) is extended to perform the computation of surface roughness of individual mountains extracted from DEMs. Accurate computation of surface roughness of mountains is important as it, along with key geomorphological parameters such as mountain-belt width and valley height/width ratios, contribute to the understanding of the evolution of mountain topography (Summerfield, 1996, 2000; Miliareisis and Argialas, 2002; Miliareisis and Iliopoulou, 2004; Miliareisis, 2008).

2 The Global Digital Elevation Model (GTOPO30) of Great Basin

The DEM in Figure 1(a) shows the area of Great Basin, Nevada, USA. The area is bounded by latitude 38° 15' to 42° N and longitude 118° 30' to 115° 30'W. The DEM was rectified and resampled to 925m in both x and y directions. The DEM is a Global Digital Elevation Model (GTOPO30) and was downloaded from the USGS GTOPO30 website (<http://edcwww.cr.usgs.gov/landdaac/gtopo30/gtopo30.html>). GTOPO30 DEMs are available at a global scale, providing a digital representation of the Earth's surface at a 30 arc-seconds sampling interval. The land data used to derive GTOPO30 DEMs are obtained from digital terrain elevation data (DTED), the 1-degree DEM for USA and the digital chart of the world (DCW). The accuracy of GTOPO30 DEMs varies by location according to the source data. The DTED and the 1-degree dataset have a vertical accuracy of $\pm 30\text{m}$ while the absolute accuracy of the DCW vector dataset is $\pm 2000\text{m}$ horizontal error and $\pm 650\text{m}$ vertical error (Miliareisis and Argialas, 2002).

3 Mountain Extraction

Mountains are the portions a terrain that are sufficiently elevated above the surrounding land (greater than 300 to 600m) and have comparatively steep sides. In a mountain, two parts are distinctive:

- 1) The summit, the highest point (the peak) or the highest ridges
- 2) The mountainside, the part of a mountain between the summit and the foot (Bates and Jackson, 1987).

The mapping of mountains is generally performed manually through fieldwork and visual interpretation of topographic maps, which is a time consuming and labor intensive activity. In recent times, extraction techniques have evolved from manual through computer assisted to automated methods with DEMs as the input data. In seeking the efficient extraction of mountains from DEMs, various algorithms have been proposed (Graff and User, 1993; Miliareisis and Argialas, 1999; Miliareisis, 2000; Dinesh, 2006).

The mountains of the DEM of Great Basin are extracted using the mathematical morphological based algorithm proposed in Dinesh (2006). First, ultimate erosion is performed on the DEM to extract the peaks of the DEM. Conditional dilation is performed on the extracted peaks to obtain the mountains of the DEM. A total of 14 distinct individual mountains objects are extracted from the DEM (Figures 1(b) and 1(c)).

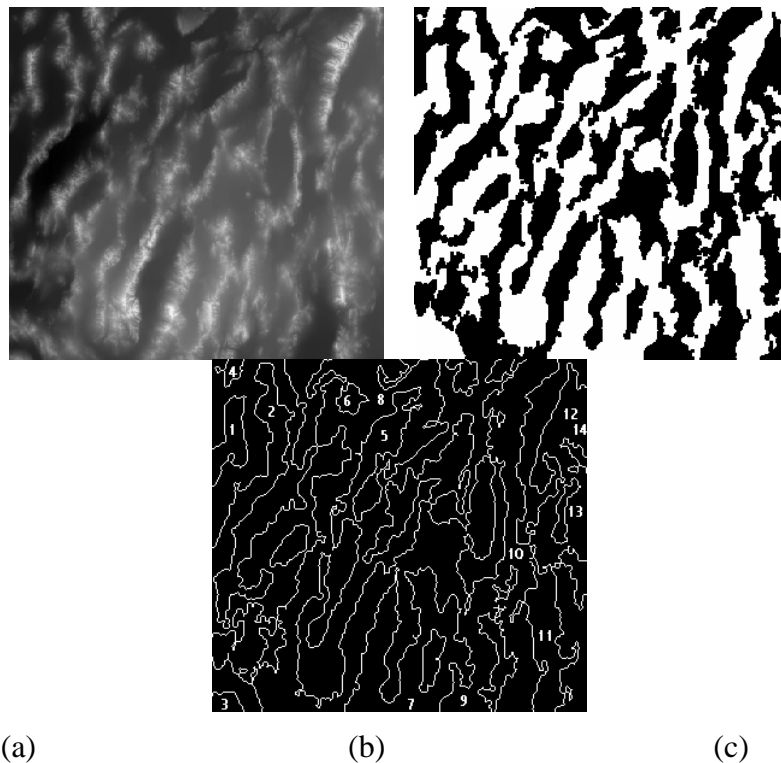


Figure 1: Extraction of mountains from GTOPO30 DEM of Great Basin. (a) The GTOPO30 DEM of Great Basin. The elevation values of the terrain (minimum 1005 meters and maximum 3651 meters) are rescaled to the interval of 0 to 255 (the brightest pixel has the highest elevation). The scale is approximately 1:3,900,000. (b) The extracted mountains. (c) A total of 14 individual mountains objects are identified using connected component labeling (Pitas, 1993).

4 Generation of Multiscale DEMs using the Lifting Scheme

Feature detection and characterization often need to be performed at different of scales measurement. Wood (1996a, b) shows that analysis of a location at multiple scales allows for a greater amount of information to be extracted from a DEM about the spatial characteristics of a feature. The term scale refers to combination of both spatial extent, and spatial detail or resolution (Goodchild and Quattrochi, 1997; Tate and Wood, 2001). A number of research efforts have been conducted to characterize geomorphological features, such as drainage and ridge networks, catchments, and mountains, using the variation in the spatial resolution over which these features are defined.

In this paper, multiscaling is performed using the lifting scheme (Sweldens, 1996, 1997). The lifting scheme is a flexible technique that has been used in several different settings, for easy construction and implementation of traditional wavelets and of second generation wavelets, such as spherical wavelets. Although several the lifting scheme has proven to be a powerful multiscale analysis tool in image and signal processing (Claypoole and Baraniuk, 2000; Starck, 2002), its implementation to DEMs has yet to capture the desired attention. Lifting consists of the following three basic operations:

Step 1: Split

The original data set $x[n]$ is divided into two disjoint subsets, even indexed points $x_e[n]=x[2n]$, and odd indexed points $x_o[n]=x[2n+1]$.

Step 2: Predict

The odd and even subsets are often highly correlated. This correlation structure typically local and hence, it is possible to accurately predict the wavelet coefficients $d[n]$ as the error in predicting $x_o[n]$ from $x_e[n]$ using the prediction operator P :

$$d[n] = x_o[n] - P(x_e[n])$$

(1)

where

$$P(x_e[n]) = \frac{1}{2}(x_e[n] + x_e[n+1])$$

(2)

Step 3: Update

Scaling coefficients $c[n]$ that represent a coarse approximation to the signal $x[n]$ are obtained by combining $x_e[n]$ and $d[n]$. This is accomplished by applying an update operator U to the wavelet coefficients and adding to $x_e[n]$:

$$c[n] = x_e[n] + U(d[n])$$

(3)

where

$$U(d[n]) = \frac{1}{4}(d[n-1] + d[n+1])$$

(4)

These three steps form a lifting stage. The lifting scheme scans 2D images row-by-row. Using a DEM as the input, an iteration of the lifting stage generates the complete set of multiscale DEMs $c_r[n]$ and the elevation loss caused by the change of scale $d_r[n]$.

Multiscale DEMs of the Great Basin region are generated by implementing the lifting scheme on the DEM of Great Basin using scales r of 1 to 20. As shown in Figure 2, as the scale increases, the merge of small regions into the surrounding grey level regions increases, causing removal of fine detail in the DEM. As a result, the generated multiscale DEMs possess lower resolutions at higher degrees of scaling.

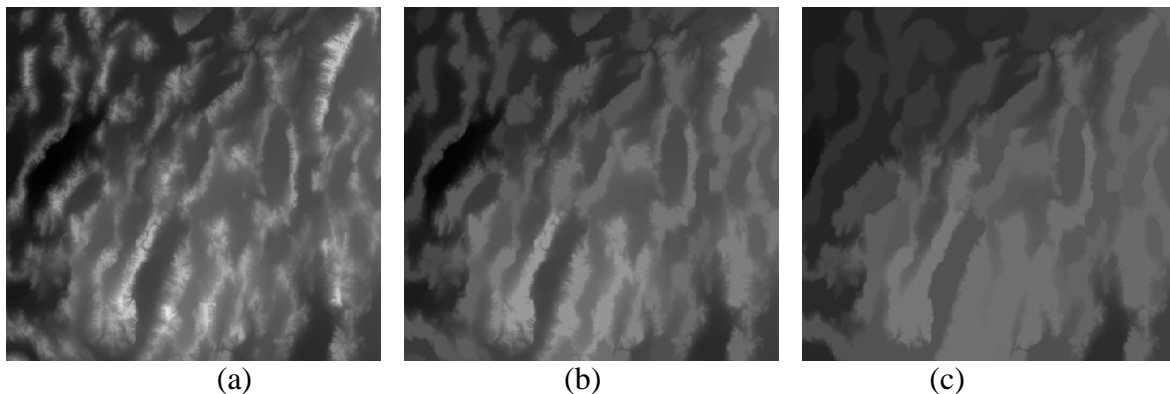


Figure 2: Multiscale DEMs generated using scales of (a) 3 (b) 10 (c) 20.

The fine detail in DEMs represents crenulations, which are used to extract hydrological features from DEMs. Convex crenulations are used to extract ridge networks while concave crenulations are used to extract drainage networks (Gilbert, 1909; Howard, 1994; Rodríguez-Iturbe and Rinaldo, 1997). The distribution of convex and concave regions in a terrain indicates the surface roughness of the terrain. The removal of convex and concave regions from the terrain during the multiscaling process results in the terrain becoming smoother. It is observed in Figure 3 that as the scale increases, the area of individual convex and concave regions increase, while the number of individual convex and concave regions decrease. This observation indicates that the development of an accurate surface roughness parameter requires an accurate quantification of a region's convexity/concavity over varying scales, distinguishing between shallow and deep incisions of the terrain.

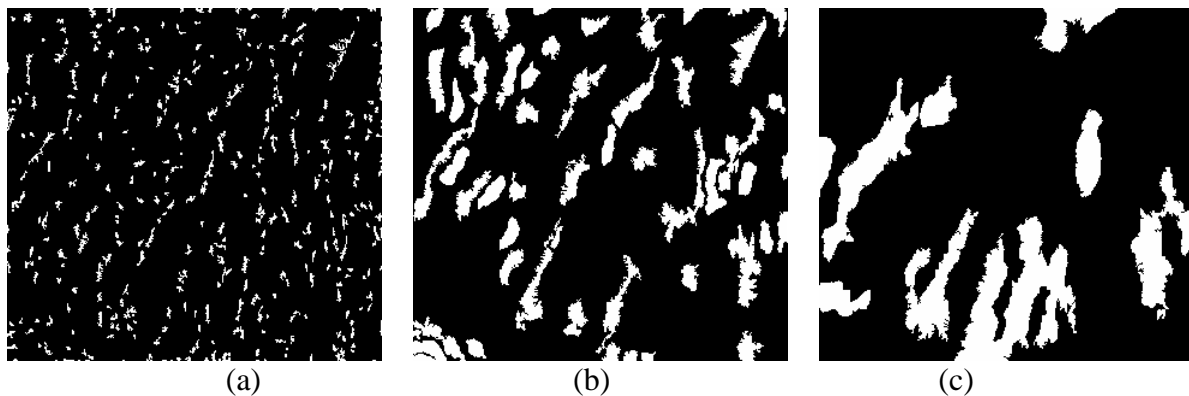


Figure 3: Mask of pixels modified during the multiscaling process for the corresponding multiscale DEMs in Figure 2. This indicates the convex and concave regions removed from the DEM during the multiscaling process.

5 Computation of Surface Roughness of Individual Mountain Objects

The procedure proposed to perform the computation of surface roughness of the individual mountain objects is demonstrated using the first mountain object (Figure 4). The mask of pixels modified in the each mountain object at each scale (Figure 6) is computed by performing the intersection operation between the mountain object and the mask of pixels modified at each scale. The normalized probability functions of the mountain object $s(r)$ are computed as the ratio of the area of pixels modified in the mountain object at each scale $S(r)$ to the area of the mountain object S_0 .

$$s(r) = S(r)/S_0$$

(5)



Figure 4: The first mountain object.

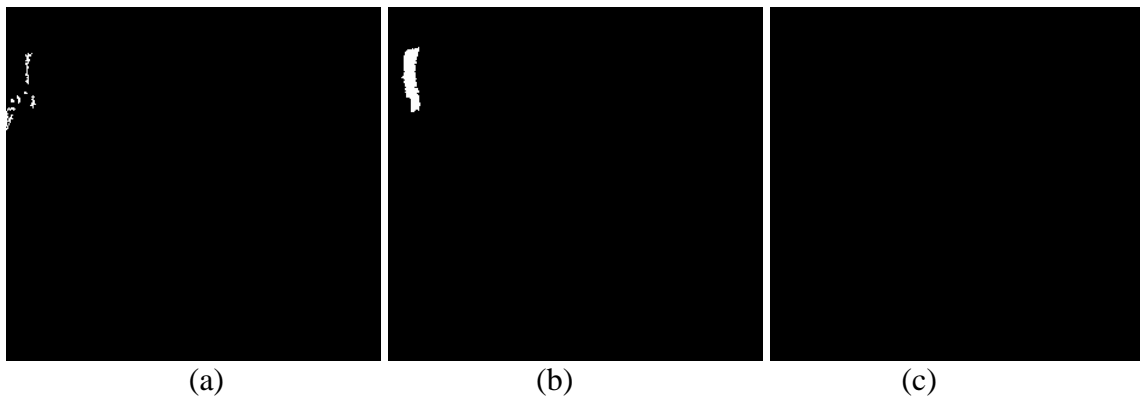


Figure 5: The mask of pixels modified in the first mountain object during the multiscaling process for the corresponding multiscale DEMs in Figure 3. This indicates the convex and concave regions removed from the mountain object during the multiscaling process.

A larger value of $s(r)$ indicates a larger area of convex and concave regions removed at scale r . As observed in Figure 7, $s(r)$ increases as the scale is increased, indicating the importance of multiscale analysis in surface roughness computation. At scales 19 and above, $s(r)$ has a value of 0, indicating that all convex and concave regions in the mountain object have been removed.

The computed values of $s(r)$ are used to compute average roughness of the mountain object H , which indicates surface roughness of the mountain object due to the convex and concave region distribution averaged over the area of the mountain object. H is computed using the following equation, which is due to Maragos (1989):

$$H = \sum_{r=1}^{20} s(r) \log s(r)$$

(6)

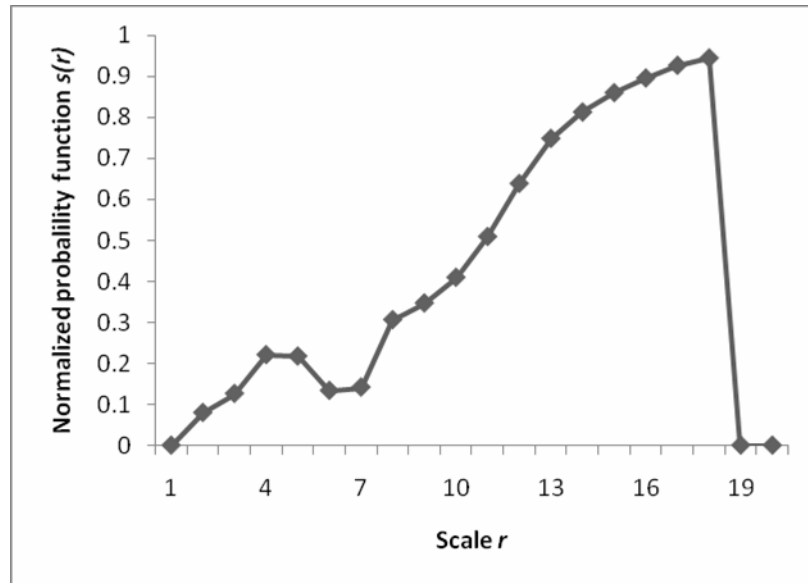


Figure 7: Plot of the normalized probability functions of the first mountain object $s(r)$ against the scale r .

6 Results and Analysis

H for the first mountain object is computed to be 1.79. In order to demonstrate the importance of scale-independent surface roughness, the surface roughness of the first mountain object across the varying scales of measurement is computed using a commonly used scale-dependent surface roughness parameter; RMS height (Brock, 1983; Hoffman and Krotkov, 1989; Bennett, 1992; Shepard et al., 2001; Li et al., 2005; Yokota et al., 2008). It is observed in Table 1 that as the scale is increased, the surface roughness of the mountain object reduces due to the reduction of fine detail in the generated multiscale DEMs. Scale-dependant roughness parameters only consider convex and concave regions at singular scales, at fixed levels of incisions, and hence, vary significantly according to scale. The methodology proposed in this paper allows for a more accurate quantification of a region's convexity/concavity over varying scales, distinguishing between shallow and deep incisions, and hence provides a more accurate surface roughness parameter.

Table 1: Surface roughness of the first mountain object over the varying scales of measurement via RMS height.

Scale	RMS height (gray level)
1	75.31
2	74.85
3	74.20
4	73.39
5	72.62
6	71.88
7	71.08
8	70.12
9	69.43
10	68.39
11	67.89
12	67.24
13	65.83
14	65.05
15	64.11
16	63.28
17	62.62
18	62.19
19	61.63
20	61.17

The proposed procedure is employed to compute the values of H for the remaining mountains objects. The computed values of S_0 and H of the extracted mountain objects are shown in Table 2. It is observed in Figure 8 that the larger the area of the mountain object, the higher is its surface roughness. This observation is consistent with the findings reported in Miliarisis and Argialas (2002).

Table 2: The computed values of S_0 and H for the individual mountain objects.

Mountain object ID	Area S_0 (pixels)	Average roughness H
1	1227	1.79
2	10422	2.65
3	1353	2.28
4	298	1.39
5	14232	2.62
6	432	2.02
7	6444	2.28
8	311	2.09
9	1119	1.71
10	219	0.88
11	3574	2.58
12	3058	2.25
13	494	1.54
14	261	1.80

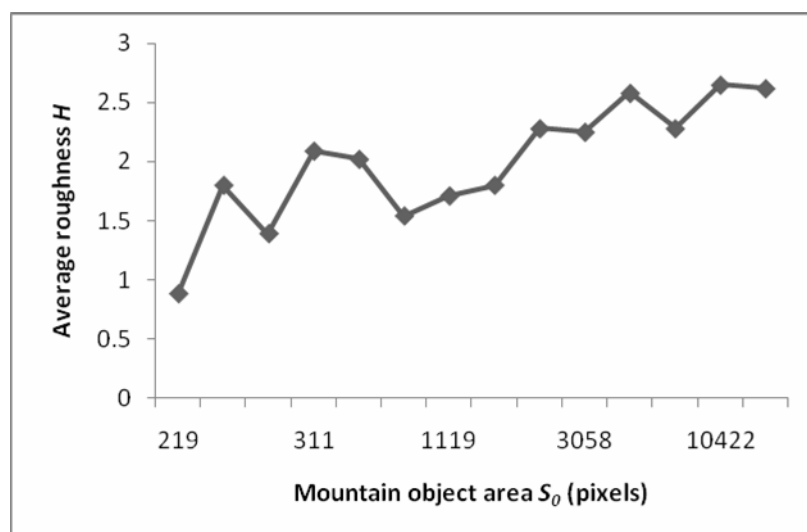


Figure 8: Plot of the area of the mountain objects S_0 against the average roughness of the mountain objects H .

4 Conclusion

In this paper, a procedure to compute the surface roughness of individual mountain objects extracted from DEMs was proposed. First, mathematical morphology was employed to extract the mountains of the DEM. The lifting scheme was employed to perform the generation of multiscale DEMs. The mask of pixels modified in the each mountain object at each scale was computed by performing the intersection operation between the mountain object and the mask of pixels modified at each scale. The normalized probability functions for each mountain object were computed as the ratio of the area of pixels modified in the mountain object at each scale to the area of the mountain object. The computed normalized probability functions were used to compute the average size of convex and concave regions in the mountain objects, and the scale-independent average roughness of the mountain objects due to the convex and concave region distribution averaged over the mountain objects. The proposed methodology allows for a more accurate quantification of a region's convexity/concavity over varying scales, distinguishing between shallow and deep incisions of terrains, and hence provides a more accurate surface roughness parameter. It was observed that the larger the area of the mountain object, the higher is its surface roughness.

References

- 1) Bates, R.L. and J.A. Jackson (Eds.), 1987. Glossary of Geology. Alexandria, American Geological Institute, Virginia.
- 2) Bennett, J.M., 1992. Recent developments in surface roughness characterization. *Measurement Science and Technology*, 3, 1119-1127.
- 3) Brock, M., 1983. *Surface Roughness Analysis*. Brüel & Kjær Instruments Inc., Nærum, Denmark.
- 4) Campbell, B.A and J.B. Garvin, 1993. Lava flow topographic measurements for radar data interpretation, *Geophysical Research Letters*, 20(9), 831-834.
- 5) Claypoole, R.L. and R.G. Baraniuk, 2000. A multiresolution wedgelet transform for image processing, In M. A. Unser, A. Aldroubi, and A.F. Laine, (Eds.) *Wavelet Applications in Signal and Image Processing VIII*, Volume 4119 of SPIE Proceedings, 253-262.
- 6) Dabrowski, B. and Banaszkiwicz, M., 2008. Multi-rover navigation on the lunar surface. *Advances in Space Research*, 42(2), 369-378.

- 7) Dinesh, S., 2006. Extraction of mountains from digital elevation models using mathematical morphology. *GIS Development Malaysia*, 1(4), 16-19.
- 8) Dinesh, S., Fadzil, M.H.A, and Vijanth, S.A. 2008. Computation of scale-independent surface roughness via the generation of multiscale digital elevation models. *International Conference on Computer & Communication Engineering 2008 (ICCCE08)*, 13th-15th May 2008, Istana Hotel, Kuala Lumpur.
- 9) Gilbert, G.K., 1909. The convexity of geology. *Journal of Geology*, 17, 344-350.
- 10) Goodchild, M.F. and D.A. Quattrochi, 1997. Scale, multiscaling, remote sensing and GIS. In Quattrochi, D.A. and M.F. Goodchild (Eds.) *Scale in Remote Sensing and GIS*. Lewis Publishers, Boca Raton, Florida, 1-11.
- 11) Graff, L.H. and E.L. Usery., 1993. Automated classification of generic terrain features in digital elevation models. *Photogrammetric Engineering and Remote Sensing*, 59(9), 1409-1417.
- 12) Hoffman, R. and Krotkov, E., 1989. Terrain roughness measurement from elevation maps. *SPIE Vol. 1195 Mobile Robots IV*, 104-114.
- 13) Howard, A.D., 1994. A detachment-limited model of drainage basin evolution. *Water Resources Research*, 30(7), 2261-2285.
- 14) Kreslavsky, M.A and J.W. Head, 1999. Kilometer-scale slopes on Mars and their correlation with geologic units: Initial results from Mars Orbiter Laser Altimeter (MOLA) data. *Journal of Geophysical Research.*, 104(E9), 21,911-21,924.
- 15) Li, W.-H., Weeks, R. and Gillispie, 1998. Multiple scattering in the remote sensing of natural surfaces. *International Journal of Remote Sensing*, 19(9), 1725 – 1740.
- 16) Li, Z., Zhu, Q. and Gold, C., 2005. *Digital Terrain Modelling: Principles and Methodology*. CRC Press, New York.
- 17) Maragos, P., 1989. Pattern spectrum and multiscale shape representation. *IEEE Transactions on Pattern Analysis and Machine Intelligence*, 11 (7), 701-716.
- 18) Miliareisis, G. C., 2000. The DEM to mountain transformation of Zagros Ranges. 5th International Conference on GeoComputation, 23-25 of August 2000, University of Greenwich.
- 19) Miliareisis G., 2008. Quantification of terrain processes. *Lecture Notes in Geoinformation & Cartography*, Vol. XIV, 13-28.
- 20) Miliareisis, G.C. and D.P. Argialas, 1999. Segmentation of physiographic features from Global Digital Elevation Model/GTOPO30. *Computers & Geosciences*, 25 (7), 715-728.

- 21) Miliareisis, G.C., and D.P. Argialas, 2002. Quantitative representation of mountain objects extracted from the Global Digital Elevation Model (GTOPO30). *International Journal of Remote Sensing*, 23 (5), 949-964.
- 22) Miliareisis G. and Illiopoulou P., 2004. Clustering of Zagros Ranges from the Globe DEM representation. *International Journal of Applied Earth Observation & GeoInformation* , 5(1), 17-28.
- 23) Miller, L.S. and C.L. Parsons, 1990. Rough surface scattering results based on bandpass autocorrelation forms. *IEEE Transactions on Geoscience and Remote Sensing*, 28, 1017-1021.
- 24) Nikora, V., 2005. High-order structure functions for planet surfaces: A turbulence metaphor. *IEEE Transactions on Geoscience and Remote Sensing*, 2(3), 362-365.
- 25) Pitas, I., 1993. *Digital Image Processing Algorithms*. Prentice Hall, London.
- 26) Rodríguez-Iturbe, I. and A. Rinaldo, 1997. *Fractal River Basins: Chance and Self-Organization*. Cambridge University Press, New York.
- 27) Shepard, M.K., B.A. Campbell, M.H. Bulmer, T.G. Farr, L.R. Gaddis and J.J. Plaut, 2001. The roughness of natural terrain: A planetary and remote sensing perspective. *Journal Geophysical Research*, 106 (E12), 32,777-32,795.
- 28) Stone, R. and J. Dugundji, 1965. A study of microrelief: Its mapping, classification and quantification by means of a Fourier analysis. *Engineering Geology*, 1(2), 89-187.
- 29) Summerfield, M., 1996. *Global Geomorphology*. Longman, Essex.
- 30) Summerfield, M. (Ed.), 2000. *Geomorphology and Global Tectonics*. John Wiley & Sons, New York.
- 31) Sweldens, W., 1996. The lifting scheme: A custom-design construction of biorthogonal wavelets. *Applied Computational Harmonics and Analysis*, 3(2), 186-200.
- 32) Sweldens, W., 1997. The lifting scheme: A construction of second generation wavelets. *Journal of Mathematical Analysis*, 29(2), 511-546.
- 33) Tate, N. and J. Wood, 2001. Fractals and scale dependencies in topography. In Tate, N. and P. Atkinson (Eds.). *Modelling scale in geographical information science*. Wiley, Chicester, 35-51.
- 34) Tay, L. T., B.S.D. Sagar and H.T. Chuah, 2005a. Derivation of terrain roughness indicators via granulometries. *International Journal of Remote Sensing*, 24(3), 573-581.
- 35) Turcotte, D.L., 1997. *Fractals and Chaos in Geology and Geophysics*. Cambridge University Press, New York.

- 36) van Zyl, J.J., C.F. Burnette and T.G. Farr, 1991. Inference of surface power spectra from inversion of multifrequency polarimetric radar data. *Geophysical Research Letters*, 18(9), 1787-1790.
- 37) Wilcox, B. and D. Gennery, 1987. A Mars rover for the 1990's. *Journal of the British Planetary Society*, 40(10), 484-488.
- 38) Wood, J., 1996a. Scale-based characterization of digital elevation models. In Parker, D. (Eds.) *Innovation in GIS 3*. Taylor & Francis, London, 163-175.
- 39) Wood, J., 1996b. The geomorphological characterization of digital elevation models, PhD Thesis, Department of Geography, University of Leicester, Leicester.
- 40) Yokota, Y., Haruyama, J., Honda, C., Morota T., Ohtake, M., Kawasaki, H., Hara, S., Hioki, K and the LISM Working Group, 2008. Lunar topography: Statistical analysis of roughness next term on a kilometer scale. *Advances in Space Research*, 42(2), 259-266.